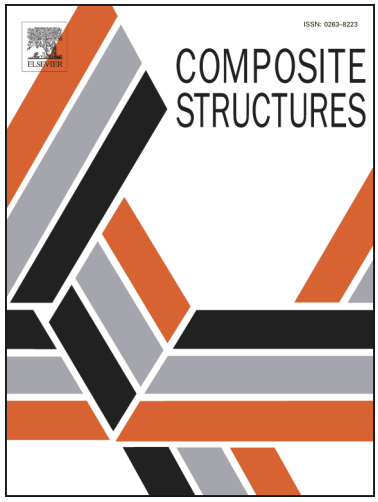

Design optimization of foam-reinforced corrugated sandwich beams

Bin Han, Ke-Ke Qin, Bo Yu, Qian-Cheng Zhang, Chang-Qing Chen, Tian Jian Lu

PII: S0263-8223(15)00317-7
DOI: http://dx.doi.org/10.1016/j.compstruct.2015.04.022
Reference: COST 6370

To appear in: *Composite Structures*

Please cite this article as: Han, B., Qin, K-K., Yu, B., Zhang, Q-C., Chen, C-Q., Lu, T.J., Design optimization of foam-reinforced corrugated sandwich beams, *Composite Structures* (2015), doi: http://dx.doi.org/10.1016/j.compstruct.2015.04.022

Design optimization of foam-reinforced corrugated sandwich beams

Bin Han[1,2], Ke-Ke Qin[1,2], Bo Yu[1,2], Qian-Cheng Zhang[1,2], Chang-Qing Chen[3], Tian Jian Lu[1,2*]

[1]*MOE Key Laboratory for Multifunctional Materials and Structures*
Xi'an Jiaotong University, Xi'an 710049, China
[2] *State Key Laboratory for Mechanical Structure Strength and Vibration*
Xi'an Jiaotong University, Xi'an 710049, China
[3]*Department of Engineering Mechanics, CNMM & AML*
Tsinghua University, Beijing 100084, China

Abstract

A combined analytical and numerical study is carried out for the structural stiffness, collapse strength and minimum mass design of foam-filled corrugated sandwich beams under transverse three-point bending. Both close-celled aluminum foam and polymer foam as the filling material are considered. Based upon a micromechanics-based model, effective elastic constants of foam-filled corrugations are derived using the homogenization method. To analytically predict the initial collapse strength, six different failure modes are considered, with the effect of loading platen width accounted for. Finite element simulations are performed to validate the analytical predictions, with good agreement achieved. Minimum mass design is obtained as a function of structural strength, and the influence of foam material and loading platen width is quantified. The structural efficiency of foam filling to reinforce the sandwich is assessed on the basis of equal mass and the underlying mechanisms explored. It is shown that polymer foam-filled corrugations are more weight efficient than unfilled ones of equal mass.

***Keywords*:** Foam-reinforced corrugated sandwich; Three-point bending; Analytical model; Minimum mass

1. Introduction

By mingling the advantageous attributes of stochastic foams and periodic lattices, hybrid-cored sandwich structures can be constructed for high stiffness, strength and energy absorption. Such hybrid sandwich cores include pin-reinforced foams [1-4], polymer foam-filled polymer lattices [5,6], polymer foam-filled fibre reinforced composite lattices [7,8], polymer foam-filled metallic lattices [9,10], and metallic foam-filled metallic lattices [11-13]. Existing studies focused mainly on the out-of-plane compression behavior of these novel structures, while only a few concerned about their bending performance [14-17].

* Corresponding author: tjlu@mail.xjtu.edu.cn (T. J. Lu)

Among the hybrid foam-lattice cores studied thus far, metallic corrugations filled with either polymer or metallic foams received special attention on account of their relatively low manufacturing cost and good structural performance. Vaziri et al. [9] found numerically that sandwich plates with polymer foam-filled metallic corrugated cores can perform as well, or nearly as well, as plates of the same weight with unfilled cores in terms of: (i) basic core responses to crush, shear and stretch, (ii) clamped plate response to quasi-static punch load, and (iii) plate response to impulsive load. Using a combined experimental and theoretical study, Yan et al. [11] and Han et al. [12] studied the quasi-static uniaxial compression behavior of metallic corrugated sandwiches filled with close-celled aluminum foams, while Yu et al. [13] explored the corresponding dynamic crushing responses. It is demonstrated [11-13] that foam filling can dramatically increase the specific compression strength and specific energy absorption of corrugated sandwich cores. Subsequently, based upon mainly experimental measurements, Yan et al. [17] studied the transverse three-point bending (i.e., bending plane normal to corrugation axis, as shown in Fig. 1) behaviors of metallic corrugated sandwich beams filled with aluminum foams. While filling of aluminum foam led to dramatically increased bending stiffness and strength of the sandwich, its mass also increased considerably [17]. Under transverse three-point bending, it is uncertain whether filling a corrugated core with foam can result in a larger failure load than that of an empty core with equal mass.

As a companion study of Yan et al. [17], this article explores further the concept of foam filling to reinforce corrugated sandwiches in three-point bending, with emphasis placed upon minimum mass design, structural efficiency assessment and strengthening mechanisms analysis. In particular, different from the Yan et al. [17], the benefit of foam filling is assessed on the basis of equal mass and both aluminum and polymer foams having high porosities are considered as the filling material.

This study firstly derives analytical expressions of both the stiffness and initial collapse strength for foam-reinforced corrugated sandwich beams in transverse three-point bending. Subsequently, minimum mass designs are carried out to quantify the structural efficiency of foam-filled corrugations on the basis of equal mass. The

underlying strengthening mechanisms are explored and collapse mechanism maps constructed. Finally, finite element (FE) simulations are performed to visualize the failure modes of different foam-corrugation combinations and to validate the analytical model predictions.

2. Stiffness and strength of foam-filled corrugated sandwich beams

Consider a foam-filled corrugated sandwich beam subjected to transverse 3-point bending with span length *L* and overhang *H*, as depicted in Fig. 1. Relevant geometric variables are: face sheet thickness t_f, corrugated member thickness t, corrugated member length l, corrugation angle θ, core height c, and sandwich beam width *b*. The volume fraction λ of the corrugated members and density ρ_c of the unit cell in the sandwich core are given by:

$$\rho_c = \lambda\rho_s + (1-\lambda)\rho_f \tag{1}$$

$$\lambda = \frac{2t}{l\sin 2\theta} \tag{2}$$

where ρ_s and ρ_f represent the density of the corrugated member material and foam, respectively. Let E_s and ν denote the Young's modulus and Poisson ratio of the corrugated member material; while E_f and ν_f denote the Young's modulus and Poisson ratio of the foam.

It is assumed that the corrugated members are perfectly bonded to the face sheets and no sliding occurs when subjected to loading. It is further assumed that the corrugated members and the filling foam keep close contact with each other during deformation, even though slip may occur at the interface.

2.1. Effective elastic constants of foam-filled corrugated core

To analyze the structural response of the sandwich beam under 3-point bending, the effective elastic constants of its foam-filled core are obtained with the homogenization method. For periodic lattice cores, the homogenization method has been widely used to calculate their equivalent elastic structural performance

[14,18-20]. Using this approach, Liu et al. [19-20] derived the effective stiffness matrix of empty (unfilled) corrugated cores.

The foam-filled corrugated core may be analyzed at two different scales: (a) at the macroscale, it is treated as a homogeneous continuum solid; (b) at the microscale, the foam fillers and the corrugated members are separately considered. The derivation of micro-macro relations for such a periodic medium relies on the analysis of its representative volume element (RVE, or unit cell).

2.1.1. Homogenization of foam-filled corrugated core

As schematically shown in Fig. 2a, when subjected to a $\bar{y}-\bar{z}$ plane macroscopic strain $\mathbf{E}$, the corrugated member may be characterized as an Euler-Bernoulli beam of unit width (along the $\bar{x}$-direction), clamped at both ends, since it is typically 100~1000 times stiffer than the foam filler. For a unit cell containing two corrugated beam members surrounded by foam filling, analogous to the analysis of pin-reinforced foam cores [14], its macroscopic strain energy density may be written as:

$$G = G_b + G_f \tag{3}$$

$$G_b = \frac{1}{\Omega}\sum_{i=1}^{2}\left[\frac{1}{2}\left(\tilde{\mathbf{u}}^{(i)} + 2\tilde{\mathbf{u}}_p^{(i)}\right)^T \tilde{\mathbf{K}}^{(i)}\tilde{\mathbf{u}}^{(i)} - \tilde{g}_p^{(i)}\right] \tag{4}$$

$$G_f = (1-\lambda)\left(\frac{1}{2}C_{hjkl}^f E_{hj}E_{kl}\right) + \frac{1}{\Omega}\sum_{i=1}^{2}\tilde{g}_p^{(i)} \tag{5}$$

where G_b and G_f are the strain energy of the beam members and foam filler, respectively, Ω represents the current volume of the unit cell, superscript/subscript f denotes the foam, and $\tilde{\mathbf{u}}^{(i)}$ is the global nodal displacement vector for the *i*-th inclined beam characterized by end nodes ζ and τ (Fig. 2b):

$$\tilde{\mathbf{u}}^{(i)} = \mathbf{T}^T\tilde{\mathbf{u}}^{(i)e} \tag{6}$$

$$\tilde{\mathbf{u}}^{(i)e} = \left[w_\zeta, v_\zeta, \theta_{\zeta x}, w_\tau, v_\tau, \theta_{\tau x}\right]^{(i)T} \tag{7}$$

Here, $\tilde{\mathbf{u}}^{(i)e}$ is the nodal displacement vector under local coordinates (*y*, *z*), **T** is the transformation matrix between local and global coordinates (see Appendix), and *e* denotes values in local coordinates. The global nodal displacement vector for the *i*-th beam may be written as:

$$\tilde{\mathbf{u}}^{(i)} = \left[\Delta_1, \Delta_1, 0, 0, 0, 0\right]^{(i)T} \tag{8}$$

where Δ_1 and Δ_2 denote the projections of displacements $\mathbf{\Delta}$ of the end nodes of the inclined beam (Fig. 2a), given by:

$$\mathbf{\Delta} = \frac{c}{\sin\theta}\mathbf{E}\mathbf{N}_0 \tag{9}$$

with

$$\mathbf{E} = \begin{bmatrix} E_{22} & E_{23} \\ sym & E_{33} \end{bmatrix}, \qquad \mathbf{\Delta} = \left(\Delta_1\mathbf{m}, \Delta_2\mathbf{r}\right)^T. \tag{10}$$

Here, $\mathbf{N}_0$ is the unit vector along which the beam member is initially aligned.

In Eq. (4), $\tilde{\mathbf{u}}_p^{(i)}$ is the nodal displacement vector of the *i*-th beam induced by lateral normal stress $p^{(i)}$ (Fig. 2b), which represents the coupling effect between the beam and foam:

$$\tilde{\mathbf{u}}_p^{(i)} = \mathbf{T}^T\tilde{\mathbf{u}}_p^{(i)\mathrm{e}} \tag{11}$$

$$\mathbf{u}_p^{(i)} = \begin{bmatrix} \dfrac{\nu p^{(i)}}{E} l & 0 & 0 & 0 & 0 & 0 \end{bmatrix}^T \tag{12}$$

The effect of shear stress on the lateral surface of the beam is ignored. The strain energy contributed by lateral normal stress $p^{(i)}$ may be divided into two parts: one is related to elongation of the *i*-th beam, as calculated in Eqs. (11) and (12); the other, related to compression on beam lateral surface and represented by $\tilde{g}_p^{(i)}$ in Eqs. (4) and (5), is eliminated during summation of the total strain energy in Eq. (3).

The macroscopic deformation of the foam in a unit cell is approximately equal to that of the unit cell, as shown in Eq. (5). Therefore, with close contact assumed between beam members and foam filler, $p^{(i)}$ is assumed to be uniformly distributed

on beam lateral surface, and can be approximately calculated as:

$$p^{(i)} = n_{22}^2 \sigma_{22}^f + n_{23}^2 \sigma_{33}^f + 2 n_{22} n_{23} \sigma_{23}^f \tag{13}$$

$$\mathbf{n}_2 = \left(n_{22},\ n_{23} \right)^T, \quad \boldsymbol{\sigma}^f = \mathbf{C}^f \mathbf{E} \tag{14}$$

where $\mathbf{n}_2$ is the unit vector normal to the outer surface of the beam and the stiffness matrix $\mathbf{C}^f$ of the foam is given in Appendix.

In Eq. (4), $\tilde{\mathbf{K}}^{(i)}$ is the global stiffness matrix that satisfies the transformation between local and global coordinates:

$$\tilde{\mathbf{K}}^{(i)} = \mathbf{T}^T \mathbf{K}^{e(i)} \mathbf{T} \tag{15}$$

where $\mathbf{K}^{e(i)}$ is the elementary stiffness matrix of the *i*-th beam, as given in Appendix.

Let the macroscopic strain vector of the unit cell be defined as:

$$\boldsymbol{\Xi} = \left[\Xi_1 \quad \Xi_2 \quad \Xi_3 \quad \Xi_4 \quad \Xi_5 \quad \Xi_6 \right]^T = \left[E_{11} \quad E_{22} \quad E_{33} \quad 2E_{23} \quad 2E_{13} \quad 2E_{12} \right]^T \tag{16}$$

Then the effective stiffness of the unit cell may be calculated as:

$$C_{ij}^H = \frac{\partial^2 G}{\partial \Xi_i \partial \Xi_j} \tag{17}$$

where the superscript *H* denotes the homogenized effective stiffness. The $\bar{y} - \bar{z}$ plane macroscopic effective stiffness $\tilde{\mathbf{C}}^{\mathbf{H}}$ of a foam-filled corrugated core may thence be obtained using Eqs. (16) and (17), as:

$$\tilde{\mathbf{C}}^{\mathbf{H}}=\begin{bmatrix} C_{22}^{H} & C_{23}^{H} & C_{24}^{H} \\ C_{23}^{H} & C_{33}^{H} & C_{34}^{H} \\ C_{24}^{H} & C_{34}^{H} & C_{44}^{H} \end{bmatrix}$$

$$=\frac{E_s}{(1-\nu^2)}\left(\frac{t}{l}\right)\begin{bmatrix} \dfrac{\cos^3\theta}{\sin\theta} & \sin\theta\cos\theta & 0 \\ \sin\theta\cos\theta & \dfrac{\sin^3\theta}{\cos\theta} & 0 \\ 0 & 0 & \sin\theta\cos\theta \end{bmatrix}+\frac{E_s}{(1-\nu^2)}\left(\frac{t}{l}\right)^3\begin{bmatrix} \sin\theta\cos\theta & -\sin\theta\cos\theta & 0 \\ -\sin\theta\cos\theta & \sin\theta\cos\theta & 0 \\ 0 & 0 & \dfrac{(\cos^2\theta-\sin^2\theta)^2}{4\sin\theta\cos\theta} \end{bmatrix}$$

$$+\frac{E_s}{(1-\nu^2)}\left(\frac{t}{l}\right)\begin{bmatrix} 2\kappa\dfrac{\cos\theta}{\sin\theta} & \left(\kappa\dfrac{\sin\theta}{\cos\theta}+\bar{\kappa}\dfrac{\cos\theta}{\sin\theta}\right) & 0 \\ \left(\kappa\dfrac{\sin\theta}{\cos\theta}+\bar{\kappa}\dfrac{\cos\theta}{\sin\theta}\right) & 2\bar{\kappa}\dfrac{\sin\theta}{\cos\theta} & 0 \\ 0 & 0 & \psi \end{bmatrix}+(1-\lambda)\begin{bmatrix} C_{22}^{f} & C_{23}^{f} & 0 \\ C_{23}^{f} & C_{33}^{f} & 0 \\ 0 & 0 & C_{66}^{f} \end{bmatrix} \tag{18}$$

where

$$\kappa=\frac{\nu(1-\nu^2)}{E_s}\left(\sin^2\theta C_{22}^{f}+\cos^2\theta C_{23}^{f}\right) \tag{19}$$

$$\bar{\kappa}=\frac{\nu(1-\nu^2)}{E_s}\left(\sin^2\theta C_{23}^{f}+\cos^2\theta C_{33}^{f}\right) \tag{20}$$

$$\psi=\frac{4\nu(1-\nu^2)}{E_s}C_{66}^{f}\sin\theta\cos\theta \tag{21}$$

In Eq. (18), the first two terms represent separately the stiffness contribution of stretching and bending deformation mechanisms for the corrugated members, the third term represents the contribution of lateral stress due to foam filling (i.e., beam-foam coupling effect) on the deformation of corrugated members, and the fourth term represents the contribution of foam filling. When $t/l<<1$ and $E_f/E_s<<1$ (as assumed in this paper), the stiffness contributions by the bending deformation of corrugated members and the coupling effect may be neglected. Thus only the first and fourth terms in (18) remain, which is similar to the simple estimate of Vaziri et al. [9].

The homogenized effective stiffness of a foam-filled corrugated core may also be obtained when the corrugated members are modeled as Timoshenko beams, if the elementary stiffness matrix formulation of Euler-Bernoulli beam is replaced by that of Timoshenko beam. However, numerical examples show that the Euler-Bernoulli beam model is accurate enough to model the behavior of the present corrugated members. Hence, for simplicity, only results for Euler-Bernoulli beams are presented hereafter.

As mentioned by Liu et al. [19], when $t/l \ll 1$, the effective stiffness matrix obtained with simply supported beam ends is nearly identical to that obtained with clamped ends. In other words, the supporting conditions of the corrugated members have negligible influence on the macroscopic stiffness of the sandwich core.

2.2. Sandwich stiffness

The macroscopic mid-span deflection δ of a sandwich beam loaded in 3-point bending is the sum of its flexural and shear deflections [21]:

$$\delta = \frac{FL^3}{48(EI)_{eq}} + \frac{\alpha_s FL}{4(GA)_{eq}} \tag{22}$$

where $(EI)_{eq}$ and $(GA)_{eq}$ represent the equivalent flexural rigidity and equivalent shear rigidity of the sandwich beam, and α_s is the shear coefficient [22]:

$$\alpha_s = \frac{(EQ)_{eq}}{(EI)_{eq}} \frac{(GA)_{eq}}{(Gb)_{eq}} \tag{23}$$

For a lightweight sandwich beam, the face sheets have negligible contribution to its shear stiffness, and the core has negligible contribution to its bending stiffness, resulting in:

$$(EQ)_{eq} = \sum_j E_j Q_j \approx \frac{E_s b t_f d}{2} \tag{24}$$

$$(Gb)_{eq} = \sum_j G_j b_j \approx b C_{44}^H \tag{25}$$

$$(EI)_{eq} = \sum_j E_j I_j \approx \frac{E_s b t_f d^2}{2} \tag{26}$$

$$(GA)_{eq} = \sum_j G_j A_j \approx bdC_{44}^H \tag{27}$$

Here, the spacing *d* of the mid-planes of the face sheets is given by $d = c + t_f$; Q is the first moment about the neutral axis of the portion of the cross-sectional area above the neutral axis; C_{44}^H is the effective shear modulus of the sandwich core in 2-3 plane; and E_j, G_j, I_j, Q_j, b_j and A_j are the effective Young's modulus, effective shear modulus, first moment, second moment, beam width and area of the cross section of the *j*-th layer (*j* = 1,2,3), respectively. Substitution of (24)-(27) into (23) leads to $\alpha_s = 1$. Then Eq. (22) is reduced to the expression given by Allen [23].

Later in Section 4, the above analytical predictions of structural stiffness are validated against FE simulation results.

2.3. Failure initiation loads

In the present study, either polymer foam or aluminum foam is taken as the filling material, while the face sheets and the corrugated members are assumed to be made of the same metal material. For a foam-filled corrugated sandwich beam subjected to transverse 3-point bending, six different failure modes are identified: 1. *face yielding* (FY), 2. *face wrinkling* (FW), 3. *core shear with corrugated member buckling* (CSB), 4. *core shear with corrugated member yielding* (CSY), 5. *indentation with corrugated member buckling* (INDB), and 6. *indentation with corrugated member yielding* (INDY). Note that, under transverse 3-point bending, each of these failure mechanisms can occur in a foam-reinforced corrugated sandwich beam, as confirmed by FE simulations (see Section 4).

To facilitate the current theoretical analysis, planar deformation (plane strain) of the sandwich beam is assumed. Thus, the face sheets and corrugated members have effective Young's modulus $\bar{E}_s = E_s/(1-\nu^2)$ and yielding stress $\bar{\sigma}_Y = 2\sigma_Y/\sqrt{3}$, while the foam material has effective Young's modulus $\bar{E}_f = E_f/(1-\nu_f^2)$. Experimentally it was found that the elastic strain limit ε_p corresponding to the

onset of plateau stress σ_p has a value on the order of 2-4% for polymer foams and 1-2% for aluminum foams [14]. For metallic corrugated members, the yielding strain ε_Y typically falls in the range of 0.1-1%. Thus, it is reasonable to assume that the onset of yielding in corrugated members is prior to that in the foam fillers.

When failure is initiated in a foam-filled corrugated sandwich beam under 3-point bending, relevant formulae governing the six different failure modes are derived as follows, with the effect of loading platen width accounted for.

2.3.1. Face yielding

Plastic collapse of metallic face sheets occurs when the axial stress within the face sheet reaches the yielding strength $\bar{\sigma}_Y$. With the pressure under the loading platen of width a (Fig. 1) assumed uniform, the maximum moment within the sandwich beam may be written as $M = F(L - a/2)/4$, rather than $M = FL/4$. With the contribution of foam-filled corrugated core to bending strength neglected, the collapse force for *face yielding* is determined by equating the maximum bending moment to the plastic collapse moment of the section, yielding:

$$F_{FY} = \frac{4bt_f d}{L - a/2}\bar{\sigma}_Y \tag{28}$$

When the width of loading platen is neglected, implying concentrated force loading, (28) is reduced to the following classical expression [17,24]:

$$F_{FY} = \frac{4bt_f d}{L}\bar{\sigma}_Y \tag{29}$$

2.3.2. Face wrinkling

As a local elastic instability of the face sheet involving short wavelength elastic buckling, *face wrinkling* only occurs in the compressive face sheet supported by a unilateral elastic foundation (foam filling) between two neighboring corrugated members. The critical wrinkling force P_{cr} may be calculated as [25]:

$$P_{cr}=\begin{cases}2\sqrt{k\bar{E}_s I}, & \text{Simply supported ends}\\ 4\dfrac{\pi^2\bar{E}_s I}{l_f^{\,2}}+2\sqrt{k\bar{E}_s I}, & \text{Clamped ends}\end{cases} \tag{30}$$

where the elastic coefficient of the elastic foundation k, the effective wrinkling length l_f, and the second moment of face sheet I are:

$$k=\frac{\bar{E}_f b}{c},\qquad l_f=2c/\tan\theta,\quad I=\frac{bt_f^3}{12} \tag{31}$$

It follows that the wrinkling stress of the face sheet σ_{FW} is given by:

$$\sigma_{FW}=\frac{P_{cr}}{t_f b}=\begin{cases}\sqrt{\dfrac{\bar{E}_f\bar{E}}{3}\left(\dfrac{t_f}{c}\right)}, & \text{Simply supported ends}\\ \dfrac{\pi^2\bar{E}}{3}\left(\dfrac{t_f}{l_f}\right)^2+\sqrt{\dfrac{\bar{E}_f\bar{E}}{3}\left(\dfrac{t_f}{c}\right)}, & \text{Clamped ends}\end{cases} \tag{32}$$

While the simply supported condition neglects the rotational restraints at the joints and underestimates the critical load associated with local buckling, the clamped condition overestimates the critical load. For conservative estimation, the simply supported condition is employed in all subsequent analysis.

Analogous to (28), the collapse load for face wrinkling may be written as:

$$F_{FW}=\frac{4btd}{L-a/2}\sigma_{FW} \tag{33}$$

The transition from face wrinkling to face yielding is:

$$\left.\frac{t_f}{c}\right|_{cr}=\frac{3\bar{\sigma}_Y^2}{\bar{E}_s\bar{E}_f} \tag{34}$$

2.3.3. Core shear with corrugated member buckling or yielding

For a sandwich beam having thin face sheets, it is usually assumed that the shear force is carried mainly by its core. For sandwich beams with metallic face sheets, two competing modes can be expected [24], as illustrated in Fig. 3: Mode A comprises plastic hinge formation in face sheets at mid-span of the sandwich, with core shear over the whole length except for the region beneath the loading platen (L+2H-a), rather than (L+2H) [24]; Mode B consists of plastic hinge formation in face sheets

both at mid-span and at the outer supports, with core shear only over the span length excluding the region beneath the loading platen (*L*-*a*), rather than *L* [24]. On equating the external work to the internal work dissipated within the core and at plastic hinges of the face sheets, the collapse force of Mode A and Mode B for the present foam-filled sandwich beam under transverse 3-point bending may be derived as:

$$F_{CS} = \begin{cases} \dfrac{2bt_f^{\,2}}{L-a}\bar{\sigma}_Y + 2bc\Sigma_{23}^{cY}\left(1+\dfrac{2H}{L-a}\right), & \text{Mode A} \\ \dfrac{4bt_f^{\,2}}{L-a}\bar{\sigma}_Y + 2bc\Sigma_{23}^{cY}, & \text{Mode B} \end{cases} \tag{35}$$

where Σ_{23}^{cY} denotes the core shear strength. The switch from Mode A to Mode B for the overhang satisfies the relation:

$$H > \frac{1}{2}\frac{t_f^2}{c}\frac{\bar{\sigma}_Y}{\Sigma_{23}^{cY}} \tag{36}$$

In the present study, it is assumed the overhang exceeds the transition value so that failure due to core shear is by Mode B. For core shear in Mode B, two kinds of failure modes may be considered: elastic buckling and yielding of corrugated members.

For the foam-filled core, the core shear strength Σ_{23}^{cY} may be expressed as

$$\Sigma_{23}^{cY} = \frac{\lambda}{2}\sigma_c \sin(2\theta) + (1-\lambda)\sigma_{23}^{foam} \tag{37}$$

where σ_c is the collapse stress of the corrugated members and σ_{23}^{foam} is the shear stress of the filling foam given by

$$\sigma_{23}^{foam} = \frac{G_f \sigma_c}{\bar{E}_s \sin(2\theta)} \tag{38}$$

When elastic buckling occurs, the buckling stress of a corrugated member buried in the foam matrix, which is treated as a superposition of Winkler type elastic foundations [25], may be obtained as:

$$\sigma_c = \begin{cases} \sqrt{\dfrac{\bar{E}_f \bar{E}_s}{3}\dfrac{t}{c\cos\theta}}, & \text{Simply supported ends} \\ \dfrac{\pi^2 \bar{E}_s}{3}\left(\dfrac{t}{l}\right)^2 + \sqrt{\dfrac{\bar{E}_f \bar{E}_s}{3}\dfrac{t}{c\cos\theta}}, & \text{Clamped ends} \end{cases} \tag{39}$$

Thus, the collapse stress of a corrugated member with simply supported ends (as a conservative analysis) is given by:

$$\sigma_c = \begin{cases} \sqrt{\dfrac{\bar{E}_f \bar{E}_s}{3} \dfrac{t}{c\cos\theta}} & \text{if } \sigma_c \le \bar{\sigma}_Y \quad \text{corrugated member buckling} \\ \bar{\sigma}_Y, & \text{otherwise} \quad \text{corrugated member yielding} \end{cases} \tag{40}$$

For corrugated members surrounded by foam filling, the transition from buckling to yielding is:

$$\left.\frac{t}{c}\right|_{cr} = \frac{3\bar{\sigma}_Y^2 \cos\theta}{\bar{E}_s \bar{E}_f} \tag{41}$$

2.3.4. Indentation with corrugated member buckling or yielding

As shown in Fig. 4, the indentation failure involves the formation of four plastic hinges within the top face sheet adjacent to the indenter as well as compressive collapse of the underlying core [24]. Correspondingly, the collapse load of indentation is given by:

$$F_{IND} = 2bt_f \sqrt{\bar{\sigma}_Y \Sigma_{33}^{cY}} + ab\Sigma_{33}^{cY} \tag{42}$$

where Σ_{33}^{cY} is the compressive strength of the core:

$$\Sigma_{33}^{cY} = \lambda\sigma_c \sin^2\theta + (1-\lambda)\sigma_{33}^{foam} \tag{43}$$

and σ_{33}^{foam} is the compressive stress of the foam:

$$\sigma_{33}^{foam} = \frac{\bar{E}_f \sigma_c}{\bar{E}_s \sin^2\theta} \tag{44}$$

Similar to core shear failure, when elastic buckling and yielding of corrugated members are taken into account for indentation failure, Eqs. (40) and (41) are applicable to indentation. However, the stress states of the corrugated members in the failure zones of core shear and indentation are different, as shown in Figs. 3 and 4. This results in the different buckling modes of corrugated members as shown in Figs. 10d-e.

3. Minimum mass optimization and failure mechanism maps

In this section, the goal is to optimize the geometric parameters of foam-filled corrugated sandwich beams to achieve minimum mass design for a prescribed structural load index $\bar{F} = F/(bL\bar{\sigma}_Y)$.

The mass per width of the sandwich beam is:

$$W = \left(2\rho_s t_f + \rho_c c\right) L \tag{45}$$

The corresponding non-dimensional expression is defined by a mass index $\bar{W} = W/\rho_s L^2$. For convenience, relevant non-dimensional geometric and material parameters are defined as:

$$\bar{\rho}_f = \rho_f/\rho_s, \quad \bar{t}_f = t_f/c, \quad \bar{t} = t/c, \quad \bar{c} = c/L, \quad \bar{a} = a/L, \quad \bar{d} = \bar{c} + \bar{t}_f \tag{46}$$

$$\lambda = \bar{t}/\cos\theta, \quad \bar{\rho}_c = \rho_c/\rho_s = \lambda + (1-\lambda)\bar{\rho}_f \tag{47}$$

$$\bar{\sigma}_c = \sigma_c/\bar{\sigma}_Y, \quad \hat{E} = \bar{E}_f/\bar{E}_s, \quad \bar{\sigma}_{FW} = \sigma_{FW}/\bar{\sigma}_Y \tag{48}$$

It follows that:

$$\bar{\Sigma}_{23}^{cY} = \Sigma_{23}^{cY}/\bar{\sigma}_Y = \left(\frac{\lambda}{2}\sin(2\theta) + \frac{(1-\lambda)\hat{E}}{(1+\nu_f)\sin(2\theta)}\right)\bar{\sigma}_c \tag{49}$$

$$\bar{\Sigma}_{33}^{cY} = \Sigma_{33}^{cY}/\bar{\sigma}_Y = \left(\lambda\sin^2\theta + (1-\lambda)\frac{\hat{E}}{\sin^2\theta}\right)\bar{\sigma}_c \tag{50}$$

And the expressions for $\bar{W}$ and $\bar{F}$ may be rewritten as:

$$\bar{W} = 2\bar{t}_f\bar{c} + \bar{c}\,\bar{\rho}_c \qquad \text{(Sandwich mass)} \tag{51}$$

$$\bar{F}_{FY} = 4\bar{t}_f(\bar{t}_f + 1)\bar{c}^2/(1-\bar{a}/2) \qquad \text{(Face yielding)} \tag{52}$$

$$\bar{F}_{FW} = 4\bar{t}_f(\bar{t}_f + 1)\bar{c}^2\bar{\sigma}_{FW}/(1-\bar{a}/2) \qquad \text{(Face wrinkling)} \tag{53}$$

$$\bar{F}_{CS} = 4\bar{t}_f{}^2\bar{c}^2/(1-\bar{a}) + 2\bar{c}\bar{\Sigma}_{23}^{cY} \qquad \text{(Core shear)} \tag{54}$$

$$\bar{F}_{IND} = 2\bar{t}_f\bar{c}\sqrt{\bar{\Sigma}_{33}^{cY}} + \bar{a}\bar{\Sigma}_{33}^{cY} \qquad \text{(Indentation)} \tag{55}$$

3.1. Minimum mass design

To minimize $\bar{M}$, the sequential quadratic programming (SQP) algorithm coded in MATLAB is employed, subjected to the constraints that none of the failure modes

detailed in Eqs. (52)-(55) occurs. The optimization is performed by imposing limits on the following geometric parameters: $\bar{t} \geq 0.01$, $\bar{c} \geq 0.01$, $10^{\circ} \leq \theta \leq 80^{\circ}$, and $\lambda \geq 1\%$, which are so chosen for ease of fabrication.

3.1.1. Influence of foam filling

To quantify the contribution of foam filling on structural efficiency, minimum mass optimizations for corrugated sandwich beams with and without foam filling as functions of structural load index $\bar{F}$ are compared in Fig. 6. The face sheets and corrugated members are all made of 304 stainless steel, with fixed loading platen width $\bar{a} = 0.04$. To fill the interstices of the corrugated core, a series of Rohacell polymer foams with varying densities (i.e., Rohacell 31, 51, 71, 110 and 200) and one aluminum foam identical to that used by Yan et al. [17] are employed, with material properties listed in Table 1. To find the best foam that maximizes the structural efficiency, two fictitious Rohacell foams, i.e., R10 and R20 with low densities of 10 kg/m^3 and 20 kg/m^3, are additionally considered. Their elastic modulus is extrapolated using the following fitting function [26] (see also Fig. 5):

$$E_f \Big/ E_{fs} = 0.8117\left(\rho_f / \rho_{fs}\right)^{1.17} \tag{56}$$

where ρ_{fs} and E_{fs} denote the density and Young's modulus of the solid parent material of the polymer foam.

For brevity, let RC10, RC20, RC31, RC51, RC71, RC110, RC200 and AC denote corrugate-cored sandwiches filled with Rohacell 10 (R10), Rohacell 20 (R20), Rohacell 31 (R31), Rohacell 51 (R51), Rohacell 71(R71), Rohacell 110 (R110), Rohacell 200 (R200) and aluminum foam, respectively. Let Empty refers to empty corrugated sandwiches.

It is striking to find that, in terms of structural efficiency, the sandwich beams considered may be classified into two categories, as shown in Fig. 6: for sandwiches filled with foams stiffer than R51, a weaker foam enhances the structural efficiency (Fig. 6a); for sandwiches filled with foams weaker than R51, a weaker foam deteriorates the structural efficiency (Fig. 6b). Further, as shown in Fig. 6c, the

sandwich filled with R51 performs best among all the sandwich types considered.

The results of Figs. 6a-b demonstrate that, on the basis of equal mass, corrugated sandwiches filled with polymer foams (Rohacell) are structurally more efficient than empty sandwiches. In contrast, the structural efficiency of corrugated sandwiches filled with aluminum foam is inferior to that of empty sandwiches of equal mass.

Under 3-point bending, the superiority of polymer foam-filled sandwiches over empty ones is more obvious at lower load levels, which gradually diminishes as the load is increased. For heavily loaded cases (e.g., $\bar{F} > 0.006$), the empty sandwiches can even outperform those filled with polymer foams. To interpret the above phenomena, the transition of failure modes along the minimum mass optimal path is presented in Fig. 6d for each type of sandwich beam. For foams weaker than R51, the failure modes of buckling including FW, CSB, and INDB dominate at low values of $\bar{F}$. In comparison, for foams stiffer than R51, the failure modes of material yielding including FY, CSY, and INDY dominate over the whole range of $\bar{F}$.

The structural enhancement due to polymer foam filling is attributed to increased buckling resistance of face sheets or corrugated members due to the lateral support of the foam matrix. The final structural efficiency is a trade-off between mass addition and enhanced buckling resistance of constituent members, both attributed to foam filling. Hence, for buckling failures (FW, CSB, INDB), a stronger structural efficiency is achieved with denser foams due to larger strengthening effect of buckling resistance; for material yielding failures (FY, CSY, INDY), a weaker structural efficiency is achieved with denser foams, as no further strengthening is gained by increasing the foam density.

As the structural load is increased, material yielding gradually dominates. Consequently, the positive strengthening effect of foam filling on face sheets or corrugated members diminishes, while the negative effect of additional mass due to foam filling becomes prominent. As a result, the structural efficiency deceases and, at sufficiently large load levels, becomes even worse than that of empty sandwiches.

Corresponding to each minimum mass design, relevant geometric parameters

including $\bar{t}_f$, $\bar{t}$, $\bar{c}$, and θ can be obtained simultaneously. However, for brevity, the results are not presented here.

3.1.2. Influence of loading platen width

Besides the influence of foam fillers, it is also instructive to explore the effect of loading platen width on minimum weight design. In Fig. 7, selected results for RC51 sandwich beams with $\bar{a} = 0$, 0.04, 0.08, 0.12, 0.2 and 0.3 are presented.

It is seen from Fig. 7a that the normalized width of loading platen $\bar{a}$ affects significantly the structural efficiency of sandwich beams, even if when $\bar{a}$ is relatively small, and thus its effect should not be neglected. As $\bar{a}$ is increased, the RC51 sandwich becomes structurally more efficient, but the sensitivity of its minimum mass to $\bar{a}$ decreases. Correspondingly, Fig. 7b presents the transition of failure modes along the minimum mass optimal path for different values of $\bar{a}$. It is intriguing to find that: for $\bar{a} = 0$, material yielding failures (FY, CSY and INDY) dominate in the whole load range; while for larger $\bar{a}$, collapses including FW, CSB or INDB dominate low and intermediate values of $\bar{F}$, and the range of such collapses increases with increasing $\bar{a}$. This enables the foam strengthening effect of buckling resistance to cover a larger range of $\bar{F}$ for larger $\bar{a}$. Additionally, the load bearing capacity corresponding to each failure mode increases as $\bar{a}$ is increased; see Eqs. (52)-(55). This may help explain why a larger $\bar{a}$ corresponds to a better structural efficiency.

3.1.3. Influence of sandwich material make

In addition to 304 stainless steel, high strength Al alloy (see Table 1) is also considered as the parent material for face sheets and corrugated members. In this case, as shown in Fig. 8, corrugate-cored sandwiches filled with foam R110, rather than R51, perform best: for sandwiches filled with foams stiffer than R110, a weaker foam enhances the structural efficiency (Fig. 8a); while, for sandwiches filled with foams weaker than R110, a weaker foam reduces the structural efficiency (Fig. 8b). Together

with the results shown in Fig. 6, this implies that as the yielding strength/strain of the parent material for face sheets and corrugated members is increased, the density (and specific elastic modulus) of the foam filler should be increased to maximize the structural efficiency of the sandwich.

Unless otherwise stated, 304 stainless steel is used in the remaining portion of this paper.

3.2. Failure mechanism maps

Two failure mechanism maps are constructed for foam-filled corrugated sandwich beams, with fixed loading platen width of $\bar{a} = 0.04$ and fixed corrugation angle of $\theta = 65^{o}$, to explore the dependence of collapse modes on face sheet thickness $\bar{t}_f$ (normalized by core height) and core height $\bar{c}$ (normalized by span length), as shown in Fig. 9. The designs of the two maps differ only in the volume fraction of corrugated members in the core: $\lambda = 1.7\%$ for Fig. 9a, and $\lambda = 8.3\%$ for Fig. 9b. To aid the selection of minimum mass geometries, contours of $\bar{W}$ and $\bar{F}$ are also added to each map.

For $\lambda = 1.7\%$ as shown in Fig. 9a, the active failure modes are FY, FW, CSB and INDB, but CSB and INDB dominate the map. With diminishing $\bar{F}$, the trajectory of minimum mass design traces firstly along the boundary between CSB and INDB regimes (indicating simultaneous failure by core shear and indentation), then along that between FY and INDB, and finally along that between FW and FY.

For $\lambda = 8.3\%$ (see Fig. 9b), the active failure modes are FY, FW, CSY and INDY, with failures of material yielding (i.e., FY, CSY and INDY) dominating the map. A comparison with Fig. 9a reveals that, as λ is increased, the failure mode of corrugated member buckling disappears, and regimes of core shear and indentation shrink. Minimum mass designs lie along the boundary between CSY and INDY regimes, through partially the boundary between FY and INDY, and finally through FY regime.

4. Finite element simulations

4.1. Finite element model

To validate the analytical predictions presented in the previous sections, 2D finite element simulations for foam-filled corrugated sandwich beams under transverse 3-point bending are performed using the commercially available FE code ABAQUS (version 6.10). The foam material is modeled using four-node plane strain quadrilateral elements with reduced integration (CPE4R). The face sheets and corrugated members are modeled using 2-node Timoshenko beam elements (B21). As shown in Fig. 10a, the mesh is denser in the vicinities of the central loading platen and the rolling supports. The embedded element technique is invoked to simulate the mutual effect between foam matrix and corrugated members. Perfect bonding between the core and the face sheets is assumed in all cases.

In the FE model, the face sheets and corrugated members are treated as isotropic ideally plastic, modeled by the J2 flow theory. As for the foam filler, the constitutive model developed by Zhang et al. [27] for polymer foams is adopted. The loading platen and rolling supports are modeled as rigid. Contacts between the bottom face sheet and the rollers as well as between the upper face sheet and the loading platen are handled by a contact algorithm using a friction coefficient of 0.01. The calculation is performed by prescribing an increasing displacement of the loading platen at slow rate so that the whole process is quasi-static. No attempt is made to conduct a post-peak study, and the analysis is interrupted shortly after achieving the maximum load. The geometric dimensions considered for the foam-filled corrugated sandwich beams are listed in Table 2, for which all the possible failure modes mentioned in Section 2.3 are included.

4.2. Comparison of FE calculations with analytical predictions

FE simulation results for six sandwich specimens, named as A1, A2, A3, A4, B1 and B2 listed in Table 2, are obtained, which collapse by FY, FW, CSB, INDB, CSY, and INDY, respectively. The failure modes of A1, A2, A3 and A4 are presented in

Figs. 10b-e. Accordingly, the normalized load $\bar{F} = F/(bL\bar{\sigma}_Y)$ as a function of normalized loading platen displacement δ/L is plotted in Fig. 11. For comparison, analytical predictions for sandwich stiffness and strength are also included.

As shown in Table 2 and Fig. 11, the failure modes, structural stiffness and strength obtained with FE calculations are in good agreement with the analytical predictions. It is noted that the analytically predicted strengths for the failure modes are all lower than the FE calculated peak loads, for the following reasons: 1) For FY and FW, the analytical predictions neglect the strength contribution of the core; 2) For FW, CSB and INDB, the rotational constraints offered by the adjoining face sheets or core members are neglected in the buckling models; 3) For corrugated member yielding of CSY and INDY, the present FE simulations reveal that, even though the corrugated core members have yielded, the strength of the sandwich has not been fully realized so that it can withstand further load increases.

As for the failure modes, while only FY and INDY at the initial failure have been identified in the experiments for corrugated sandwiches filled with close-celled aluminum foams [17], all the possible failure modes, i.e., FY, FW, CSB, CSY, INDB, and INDY, have been explored in present FE calculations for corrugated sandwiches filled with polymer foam R51.

The great difference between foam-filled and empty corrugated sandwiches under transverse 3-point bending is mainly about the failure of the core: for empty sandwiches, only failures of corrugated members (either buckling or yielding) due to shear force are considered [28,29]; for foam-filled sandwiches, besides the corrugated member failure due to shear force (i.e., CSB and CSY), the effect of indentation stresses on corrugated member failure (INDB and INDY) has also been taken into account. For corrugated member buckling in foam-filled sandwiches, it can be found from Figs. 10d-e that: for CSB, the corrugated member buckles under shear load so that one member in a unit cell is in tension and the other buckles in compression; whereas, for INDB, the two corrugated members of one unit cell beneath the loading platen both buckle in compression. Due to the lateral support of foam filling, the face

sheets and corrugated members in a foam-filled sandwich buckle with smaller buckle wave lengths than those in an empty sandwich [28].

5. Concluding remarks

An analytical study is carried out to assess the enhancement effect of foam filling on the deformation and failure behavior of metallic corrugated sandwich beams in transverse 3-point bending. The structural stiffness, initial failure strength and failure modes predicted by analytical models are compared with the results of finite element simulations to validate the present approach. Both aluminum and polymer foams as filling material are considered.

On the basis of equal mass, the structural efficiency of corrugated sandwiches filled with aluminum foams is inferior to that of the empty ones, while those filled with polymer foams (Rohacell) are structurally more efficient than the empty ones especially at relatively low load levels. The structural enhancement due to polymer foam filling is attributed to increased buckling resistance of face sheets and corrugated members due to lateral support of foam matrix. For buckling failures (FW, CSB, INDB), a larger structural efficiency is achieved with a denser foam due to larger strengthening effect of buckling resistance. For material yielding failures (FY, CSY, INDY), the structural efficiency decreases with increasing foam density, as no further strengthening is gained by increasing the foam density. As the load is increased, the failure modes of face wrinkling and corrugated member buckling disappear, replaced by material yielding. By increasing the width of loading platen, the foam-reinforced corrugated sandwich becomes structurally more efficient.

Under 3-point bending, the best performance of a metallic corrugate-cored sandwich is achieved by filling with a foam of matching density. As the yielding strength/strain for the parent material of the face sheets and corrugated members is increased, the density (and specific elastic modulus) of the foam filler should be increased to maximize the structural efficiency of the sandwich.

Acknowledgement

This work was supported by the National Basic Research Program of China (2011CB610305), the National Natural Science Foundation of China (11472209 and 11472208), the National 111 Project of China (B06024), and the Shaanxi Province 13115 Project.

Appendix

For Euler-Bernoulli beams, the elementary stiffness matrix is:

$$\mathbf{K}^{e(i)} = \begin{bmatrix} \frac{E_s A}{l} & 0 & 0 & -\frac{E_s A}{l} & 0 & 0 \\ 0 & \frac{12E_s I}{l^3} & \frac{6E_s I}{l^2} & 0 & -\frac{12E_s I}{l^3} & \frac{6E_s I}{l^2} \\ 0 & \frac{6E_s I}{l^2} & \frac{4E_s I}{l} & 0 & -\frac{6E_s I}{l^2} & \frac{2E_s I}{l} \\ -\frac{E_s A}{l} & 0 & 0 & \frac{EA}{l} & 0 & 0 \\ 0 & -\frac{12E_s I}{l^3} & -\frac{6E_s I}{l^2} & 0 & \frac{12E_s I}{l^3} & -\frac{6E_s I}{l^2} \\ 0 & \frac{6E_s I}{l^2} & \frac{2E_s I}{l} & 0 & -\frac{6E_s I}{l^2} & \frac{4E_s I}{l} \end{bmatrix} \tag{A.1}$$

where A and I are the cross-sectional area and moment of inertia of the beam, respectively.

The transformation matrix between local and global coordinates for one corrugated member as shown in Fig. 2a is given by:

$$\mathbf{T} = \begin{bmatrix} \cos\alpha & \sin\alpha & 0 & 0 & 0 & 0 \\ -\sin\alpha & \cos\alpha & 0 & 0 & 0 & 0 \\ 0 & 0 & 1 & 0 & 0 & 0 \\ 0 & 0 & 0 & \cos\alpha & \sin\alpha & 0 \\ 0 & 0 & 0 & -\sin\alpha & \cos\alpha & 0 \\ 0 & 0 & 0 & 0 & 0 & 1 \end{bmatrix} \tag{A.2}$$

The elastic constants of the filling foam are:

$$C_{22}^f = C_{33}^f = \frac{(1-\nu_f)}{(1-2\nu_f)(1+\nu_f)} E_f$$

$$C_{23}^f = \frac{\nu_f}{(1-2\nu_f)(1+\nu_f)} E_f \tag{A.3}$$

$$C_{66}^f = G_f = \frac{E_f}{2(1+\nu_f)}$$

References

[1] Cartie DD, Fleck NA. The effect of pin reinforcement upon the through-thickness compressive strength of foam-cored sandwich panels. Compos Sci Technol 2003;63(16):2401-2409.

[2] Marasco AI, Cartie DDR, Partridge IK, Rezai A. Mechanical properties balance in novel Z-pinned sandwich panels: Out-of-plane properties. Compos Part A-Appl S 2006;37(2):295-302.

[3] Nanayakkara A, Feih S, Mouritz AP. Experimental analysis of the through-thickness compression properties of Z-pinned sandwich composites. Compos Part A-Appl S 2011;42(11):1673-1680.

[4] Mouritz AP. Compression properties of Z-pinned sandwich composites. J Mater Sci 2006;41(17):5771-5774.

[5] Hammetter CI, Zok FW. Compressive response of pyramidal lattices embedded in foams. ASME, J Appl Mech 2014;81(1).

[6] Ostos JB, Rinaldi RG, Hammetter CM. Deformation stabilization of lattice structures via foam addition. Acta Mater 2012;60(19):6476-6485.

[7] Zhang GQ, Wang B, Ma L, Wu LZ, Pan SD, Yang JS. Energy absorption and low velocity impact response of polyurethane foam filled pyramidal lattice core sandwich panels. Compos Struct 2014;108:304-310.

[8] Yang L, Fan HL, Liu J, Ma Y, Zheng Q. Hybrid lattice-core sandwich composites designed for microwave absorption. Mater Des 2013;50:863-871.

[9] Vaziri A, Xue Z, Hutchinson JW. Metal sandwich plates with polymer foam-filled cores. J Mech Mater Struct 2006;1(1):97-127.

[10] Yazici M, Wright J, Bertin D, Shukla A. Experimental and numerical study of foam filled corrugated core steel sandwich structures subjected to blast loading. Compos Struct 2014;110:98-109.

[11] Yan LL, Yu B, Han B, Chen CQ, Zhang QC, Lu TJ. Compressive strength and energy absorption of sandwich panels with aluminum foam-filled corrugated cores. Compos Sci Technol 2013;86:142-148.

[12] Han B, Yan LL, Yu B, Zhang QC, Chen CQ, Lu TJ. Collapse mechanisms of metallic sandwich structures with aluminum foam-filled corrugated cores. J Mech Mater Struct 2014;9(4):397-425.

[13] Yu B, Han B, Ni CY, Zhang QC, Chen CQ, Lu TJ. Dynamic crushing of all-metallic corrugated panels filled with close-celled aluminum foams. ASME, J Appl Mech 2015;81(1):47-55.

[14] Liu T, Deng ZC, Lu TJ. Analytical modeling and finite element simulation of the plastic collapse of sandwich beams with pin-reinforced foam cores. Int J Solids Struct 2008;45(18-19):5127-5151.

[15] Zhang J, Supernak P, Mueller-Alander S, Wang CH. Improving the bending strength and energy absorption of corrugated sandwich composite structure. Mater Des 2013;52:767-773.

[16] Wang L, Liu WQ, Wan L, Fang H, Hui D. Mechanical performance of foam-filled lattice

composite panels in four-point bending: Experimental investigation and analytical modeling. Compos Part B-Eng 2014;67:270-279.

[17] Yan LL, Han B, Yu B, Chen CQ, Zhang QC, Lu TJ. Three-point bending of sandwich beams with aluminum foam-filled corrugated cores. Mater Des 2014;60:510-519.

[18] Liu T, Deng ZC, Lu TJ. Design optimization of truss-cored sandwiches with homogenization. Int J Solids Struct 2006;43(25-26):7891-7918.

[19] Liu T, Deng ZC, Lu TJ. Structural modeling of sandwich structures with lightweight cellular cores. Acta Mech Sinica 2007;23(5):545-559.

[20] Liu T, Deng ZC, Lu TJ. Minimum weights of pressurized hollow sandwich cylinders with ultralight cellular cores. Int J Solids Struct 2007;44(10):3231-3266.

[21] Timoshenko SP, Gere JM. Mechanics of Materials. New York: D. Van Nostrand; 1972.

[22] Mai SP, Fleck NA, Lu TJ. Optimal design of box-section sandwich beams in three-point bending. Int J Solids Struct 2007;44(14-15):4742-4769.

[23] Allen HG. Analysis and design of structural sandwich panels. Oxford: Pergamon Press; 1969.

[24] Ashby MF, Evans AG, Fleck NA, Gibson LJ, Hutchinson JW, Wadley HNG. Metal foams: A design guide. Oxford: Butterworth-Heinemann; 2000.

[25] Han B, Xu Y, Yu B, Chen CQ, Zhang QC, Lu TJ. Foam filling radically enhances transverse shear response of corrugated sandwich plates. Mater Des 2015. In press.

[26] Arezoo S, Tagarielli VL, Petrinic N, Reed JM, Arezoo S. The mechanical response of Rohacell foams at different length scales. J Mater Sci 2011;46(21):6863-6870.

[27] Zhang J, Lin Z, Wong A, Kikuchi N, Li VC, Yee AF, Nusholtz GS. Constitutive modeling and material characterization of polymeric foams. ASME, J Eng Mater 1997;119(3):284-291.

[28] Valdevit L, Wei Z, Mercer C, Zok FW, Evans AG. Structural performance of near-optimal sandwich panels with corrugated cores. Int J Solids Struct 2006;43(16):4888-4905.

[29] Lu TJ, Hutchinson JW, Evan AG. Optimal design of a flexural actuator. J Mech Phys Solids 2001;49(9):2071-2093.

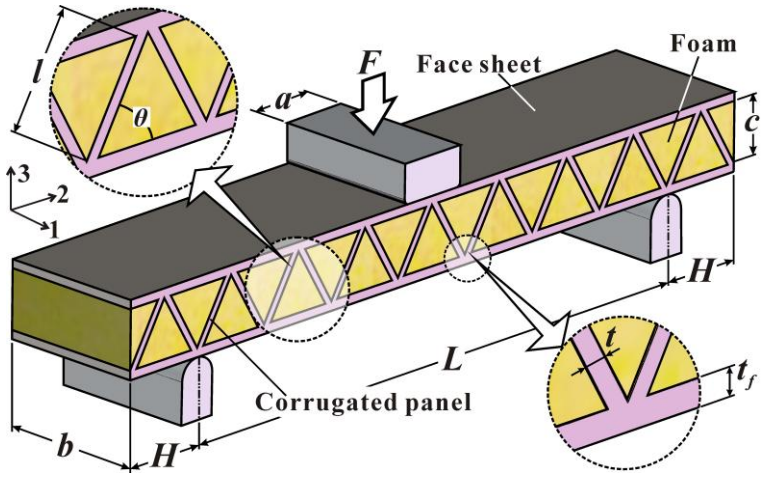

Fig. 1. Foam-reinforced corrugated sandwich beam in transverse 3-point bending.

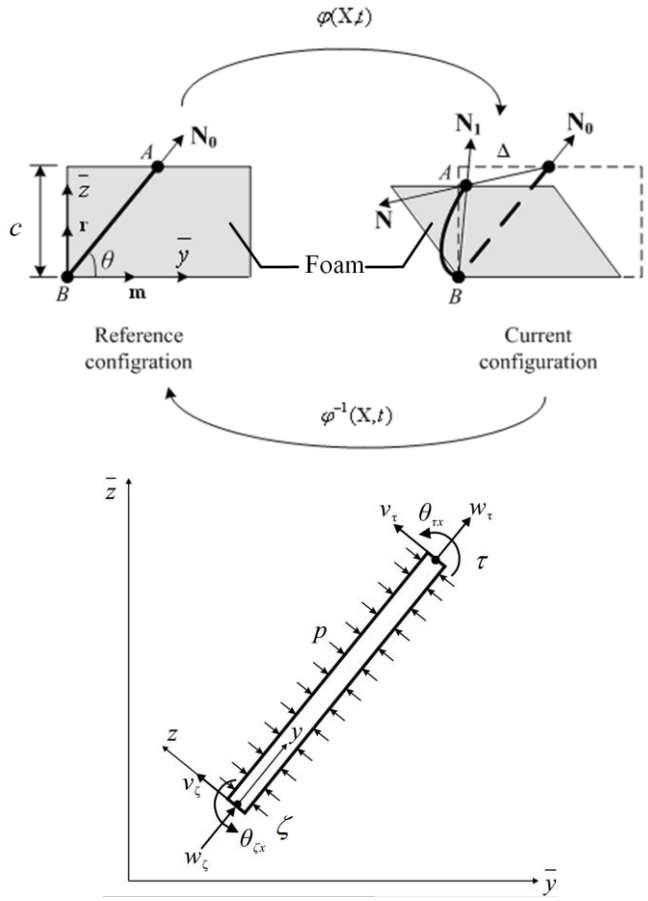

(a) (b)

Fig. 2. Homogenization of foam-filled corrugation in plane strain state: (a) kinematics of a corrugated member; (b) a corrugated member subjected to nodal forces/moments and lateral pressure.

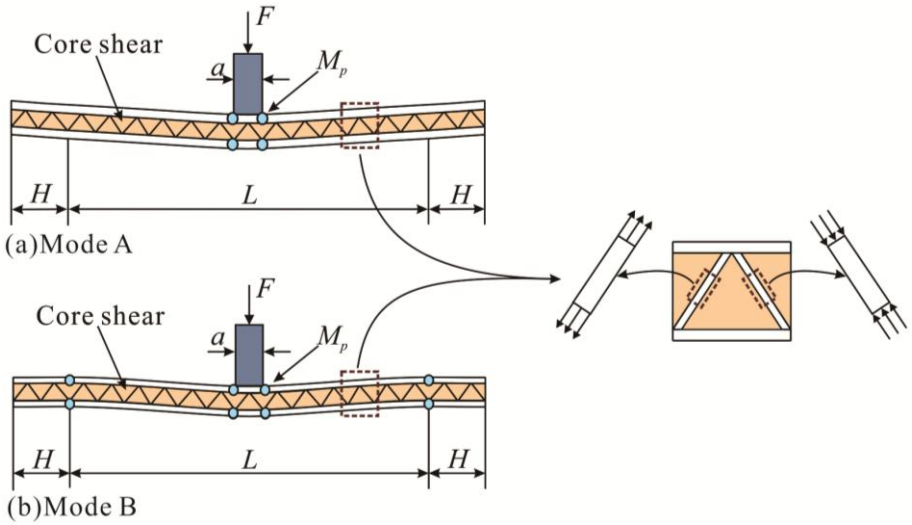

Fig. 3. Schematic of foam-reinforced corrugated core shear failure: (a) Mode A and (b) Mode B, with stress state of corrugated members in core shear highlighted.

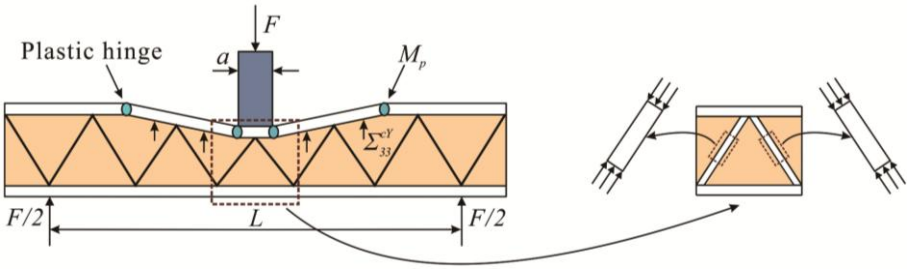

Fig. 4. Schematic of foam-reinforced core indentation failure, with stress state of corrugated members under indentation highlighted.

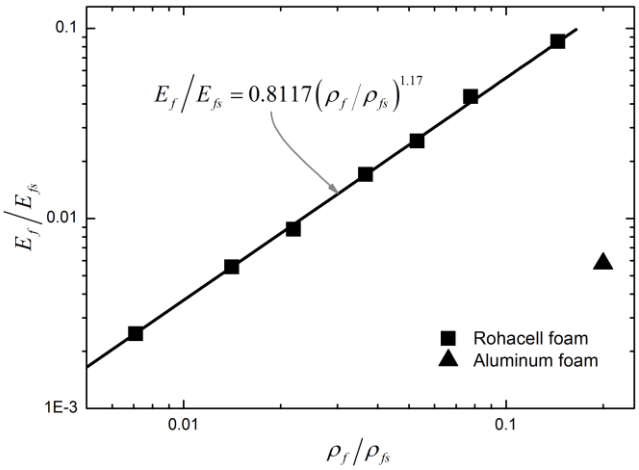

Fig. 5. Normalized elastic modulus of foam materials (used in present study) plotted as a function of their relative density.

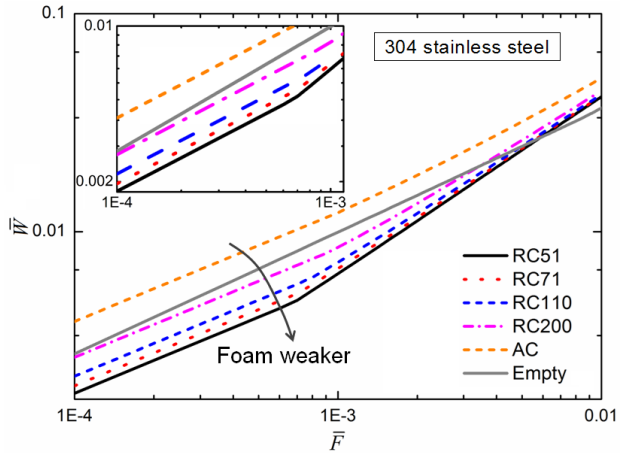
304 stainless steel
RC51
RC71
RC110
RC200
AC
Empty
Foam weaker
$\bar{W}$
$\bar{F}$

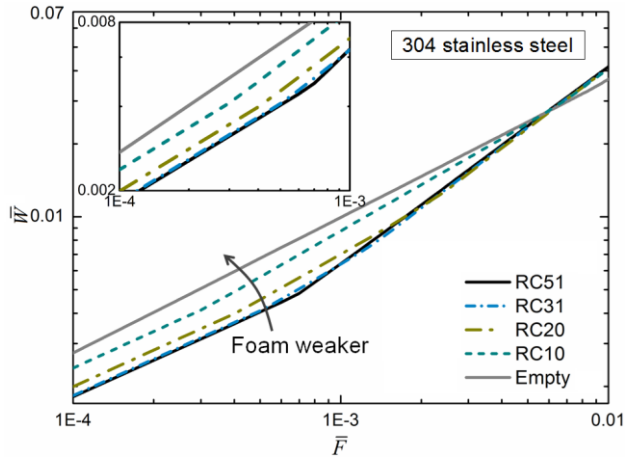
304 stainless steel
RC51
RC31
RC20
RC10
Empty
Foam weaker
$\bar{W}$
$\bar{F}$

(a) (b)

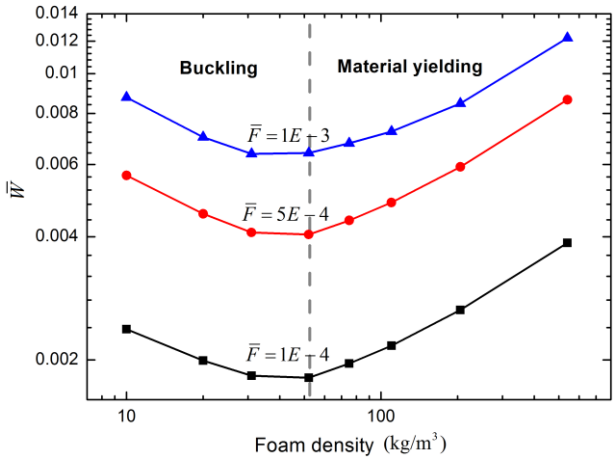
Buckling
Material yielding
$\bar{F}=1E-3$
$\bar{F}=5E-4$
$\bar{F}=1E-4$
$\bar{W}$
Foam density (kg/m^3)

(c)

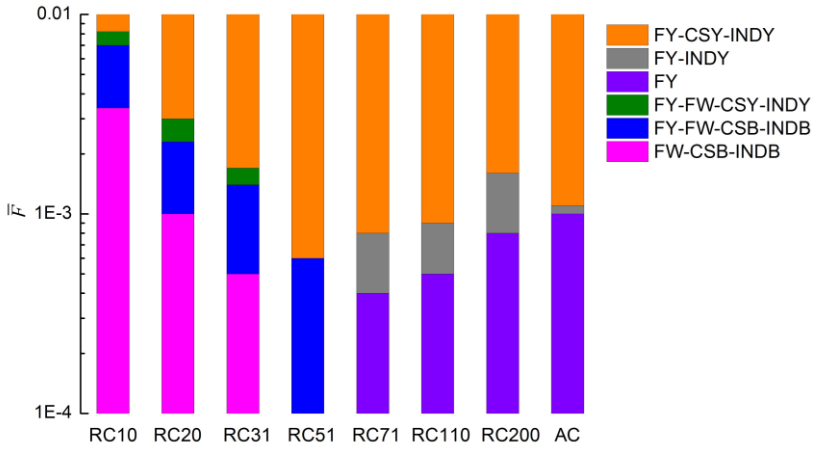

(d)

Fig. 6. Minimum mass optimization for 304 stainless steel corrugated sandwiches filled with selected foam materials ($\bar{a} = 0.04$): (a) minimum mass comparison for sandwiches filled with foams stiffer than R51; (b) minimum mass comparison for sandwiches filled with foams weaker than R51; (c) minimum mass plotted as a function of foam density for three specific structural loads; (d) transition of failure mode along optimal path. Optimization of empty corrugated sandwiches is carried out using the theoretical formulae presented by Valdevit et al. [29].

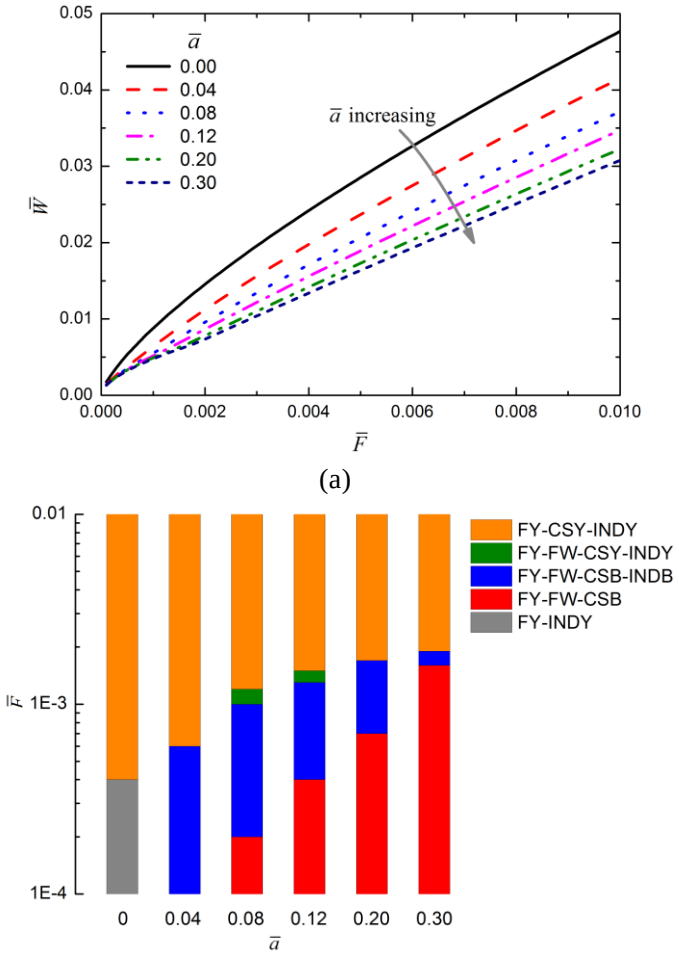

Fig. 7. Effect of loading platen width $\bar{a}$ upon minimum mass design of 304 stainless steel corrugated sandwiches filled with R51: (a) optimal path of minimum mass; (b) transition of failure mode along optimal path.

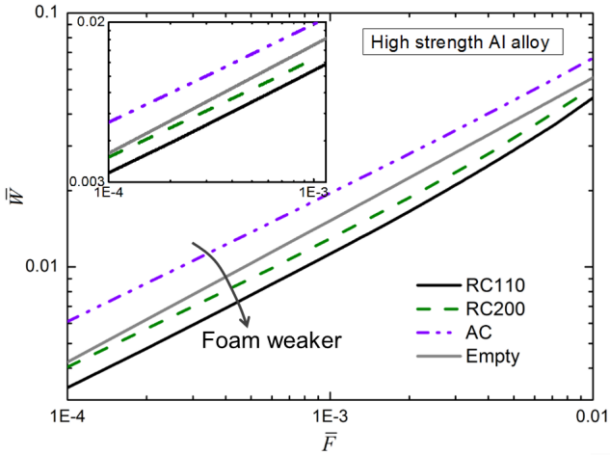

(a)

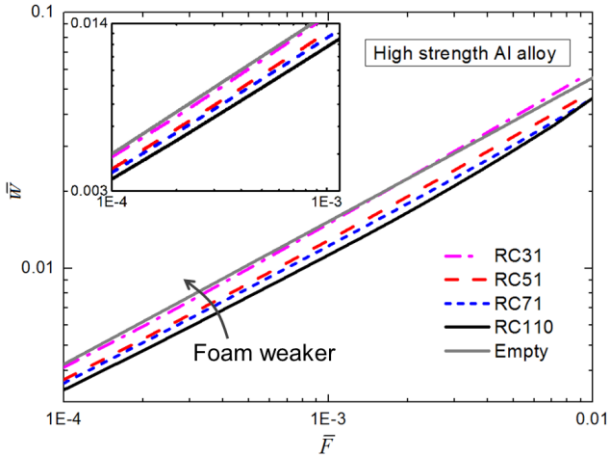

(b)

Fig. 8. Minimum mass optimization of high strength Al alloy corrugated sandwich beams filled with selected foam materials ($\bar{a} = 0.04$): (a) minimum mass comparison for sandwiches filled with foams stiffer than R110; (b) minimum mass comparison for sandwiches filled with foams weaker than R110.

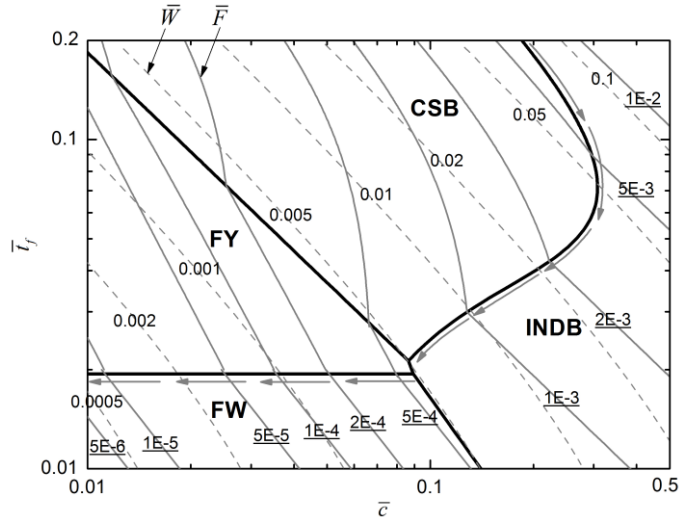

(a)

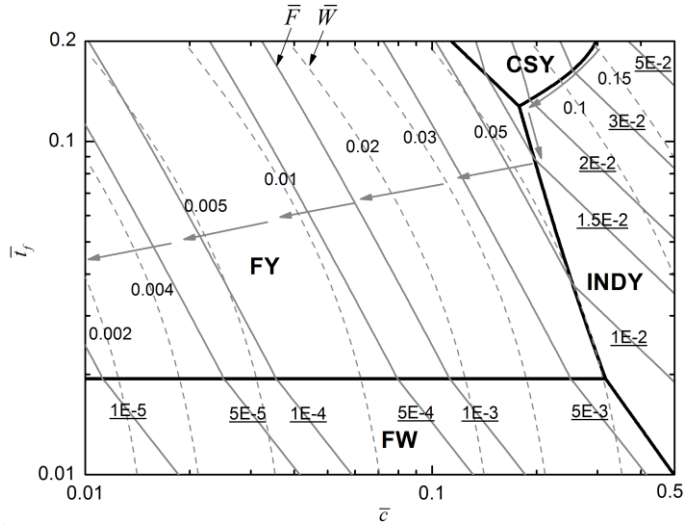

(b)

Fig. 9. Collapse mechanism map of 304 stainless steel corrugated sandwich filled with polymer foam R51 ($\theta = 65^{o}$ and $\bar{a} = 0.04$), with corrugated member volume fraction fixed at (a) $\lambda = 1.7\%$ and (b) $\lambda = 8.3\%$. Contours of $\bar{W}$ and $\bar{F}$ are also added. Gray arrows trace the path of minimum mass design with decreasing $\bar{F}$.

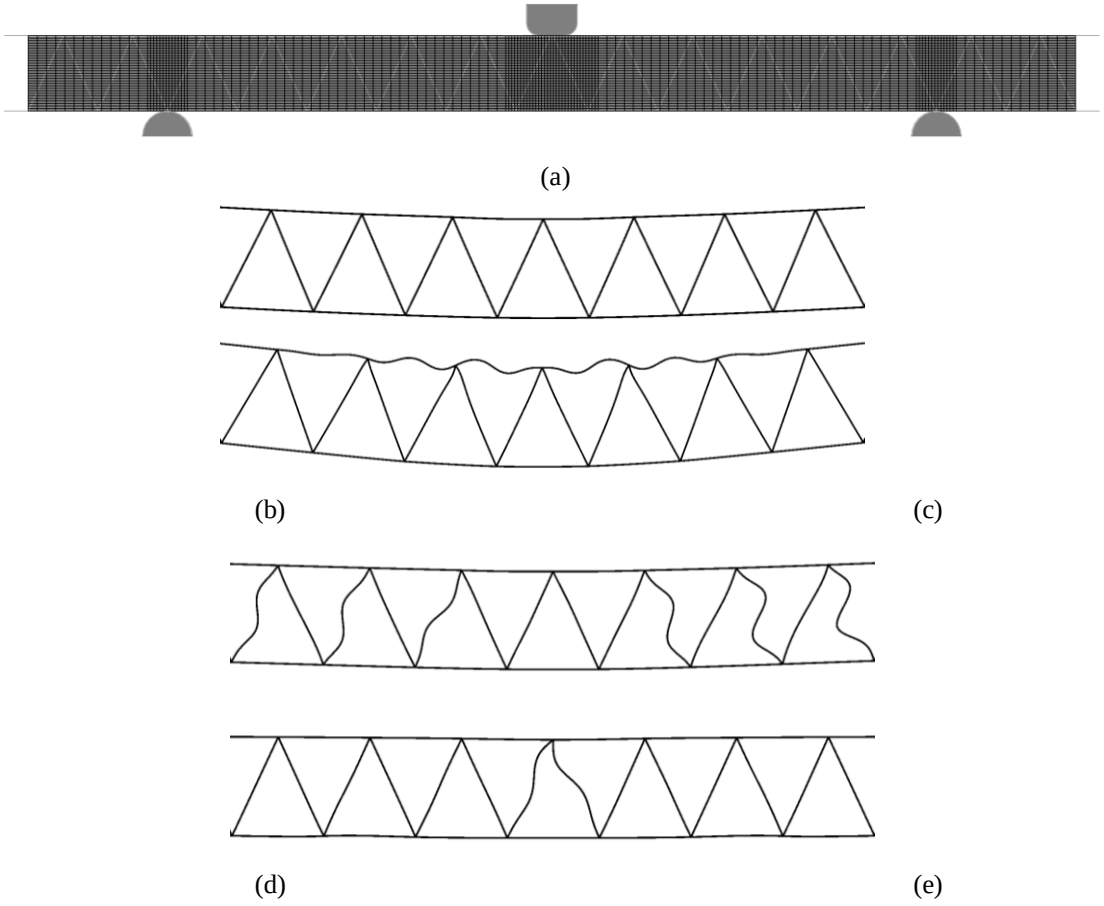

Fig. 10. Finite element simulations of foam-filled sandwich beams subjected to transverse three-point bending: (a) FE model and (b-e) typical failure modes captured by FE calculations: (b) specimen A1, failed by face yielding; (c) specimen A2, failed by face wrinkling; (d) specimen A3, failed by core shear with corrugated member buckling, and (e) specimen A4, failed by indentation with corrugated member buckling. For clarity, the simulated deformations are exaggerated by 2~5 times.

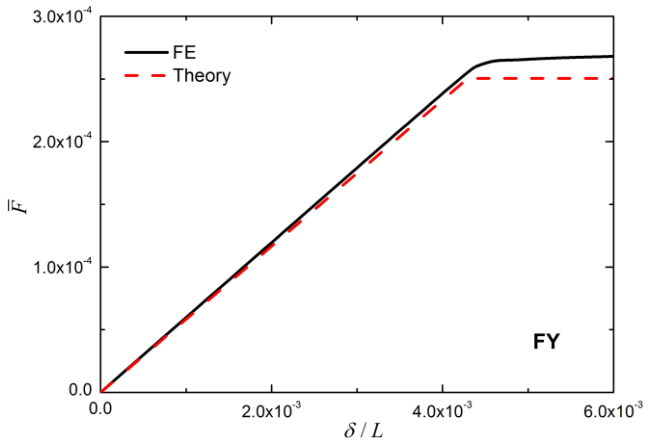
FE
Theory
FY
$\bar{F}$
δ / L
3.0x10^{-4}
2.0x10^{-4}
1.0x10^{-4}
0.0
2.0x10^{-3}
4.0x10^{-3}
6.0x10^{-3}

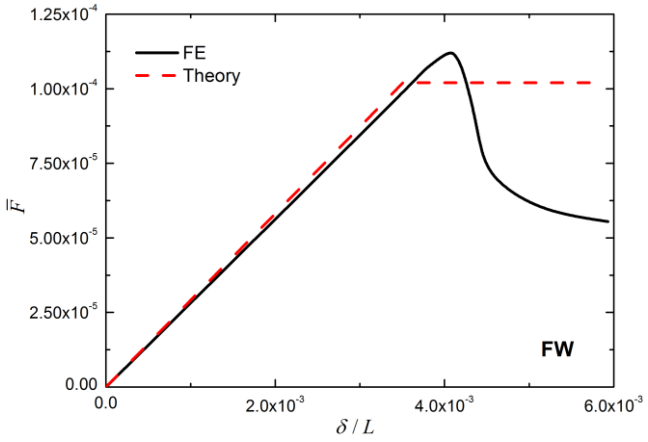
FE
Theory
FW
$\bar{F}$
δ / L
1.25x10^{-4}
1.00x10^{-4}
7.50x10^{-5}
5.00x10^{-5}
2.50x10^{-5}
0.00
0.0
2.0x10^{-3}
4.0x10^{-3}
6.0x10^{-3}

(a) (b)

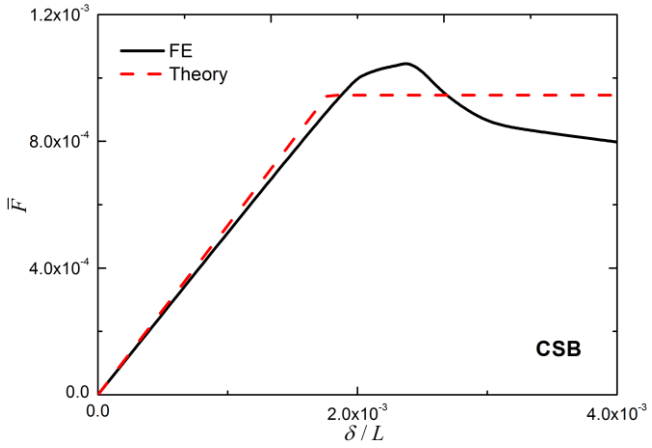
FE
Theory
CSB
$\bar{F}$
δ / L
1.2x10^{-3}
8.0x10^{-4}
4.0x10^{-4}
0.0
2.0x10^{-3}
4.0x10^{-3}

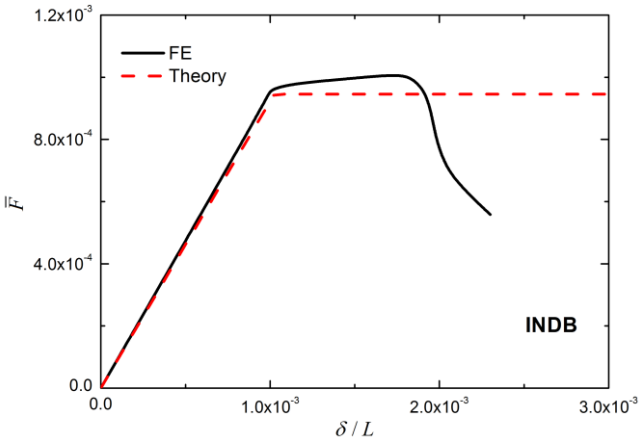

(c) (d)

Fig. 11. Quasi-static responses of foam-filled sandwich beams in transverse 3-point bending, corresponding to the failure modes of Figs. 10b-e: (a) specimen A1; (b) specimen A2; (c) specimen A3; (d) specimen A4.

Table 1: Mechanical properties of (a) foams and (b) base materials of face sheets and corrugated members.

Material	Density	Young's modulus	Poisson ratio	Initial uniaxial compressive yield stress
(a) Foam	ρ_f (g/cm^3)	E_f (MPa)	ν_f	σ_p (MPa)
Rohacell 10	0.010	10	0.3	-
Rohacell 20	0.020	23	0.3	-
Rohacell 31	0.031	36	0.2	0.4
Rohacell 51	0.052	70	0.3	0.8
Rohacell 71	0.075	105	0.25	1.7
Rohacell 110	0.110	180	0.28	3.6
Rohacell 200	0.205	350	0.17	9
Al foam	0.540	405	0.30	13.14
(b) Base material	ρ_s (g/cm^3)	E_s (GPa)	ν	σ_Y (MPa)
304 stainless steel	7.9	210	0.3	210 ($\varepsilon_Y = 0.001$)
High strength Al alloy	2.7	70	0.33	490 ($\varepsilon_Y = 0.007$)

Note: Mechanical properties of polymer foam Rohacell series are obtained from manufacturer (ROHM) data sheets. Properties of Rohacell 10 and 20 (marked in italic) are extrapolated using fitting function Eq. (56), as shown in Fig. 5. Al foam refers to close-celled aluminum foam used in Yan et al. [17]. Both 304 stainless steel and high strength Al alloy in present study are treated as elastic-perfectly plastic materials.

Table 2: Comparison of analytical predictions and finite element simulations of foam-filled corrugated sandwich beams under transverse 3-point bending.

Specimen	t_f/c	c/L	L (mm)	θ	λ (%)	Analytical failure mode	FE failure mode	FE peak load F (kN)	Analytical/ FE peak load
A1	0.03	0.05	300	65^o	1.7	FY	FY	19.5	0.934
A2	0.012	0.05	300	65^o	1.7	FW	FW	8.2	0.910
A3	0.04	0.13	150	65^o	1.7	CSB	CSB	38.2	0.901
A4	0.02	0.2	150	65^o	1.7	INDB	INDB	36.7	0.936
B1	0.15	0.17	150	65^o	8.3	CSY	CSY	725.8	0.873
B2	0.05	0.25	150	65^o	8.3	INDY	INDY	559.2	0.852

Note: The material make of both the face sheets and corrugated members is 304 stainless steel. The foam filler is Rohacell 51. The loading platen width is fixed at $\bar{a} = 0.04$ (normalized by span length).